Inorganic Chemistry

Article

pubs.acs.org/IC

Mixture of Fuels Approach for the Synthesis of $SrFeO_{3-\delta}$ Nanocatalyst and Its Impact on the Catalytic Reduction of Nitrobenzene

Akula Naveenkumar,[†] Praveena Kuruva,[‡] Chikkadasappa Shivakumara,[†] and Chilukoti Srilakshmi*[,†]

[†]Solid State and Structural Chemistry Unit (SSCU), and [‡]Materials Research Centre (MRC), Indian Institute of Science (IISc), Bangalore 560012, Karnataka, India

Supporting Information

ABSTRACT: A modified solution combustion approach was applied in the synthesis of nanosize $SrFeO_{3-\delta}$ (SFO) using single as well as mixture of citric acid, oxalic acid, and glycine as fuels with corresponding metal nitrates as precursors. The synthesized and calcined powders were characterized by Fourier transform infrared spectroscopy (FT-IR), X-ray diffraction (XRD), thermogravimetric analysis and derivative thermogravimetric analysis (TG-DTG), scanning electron microscopy, transmission electron microscopy, N_2 physisorption methods, and acidic strength by *n*-butyl amine titration methods. The FT-IR spectra show the lower-frequency band at 599 cm^{-1} corresponds to metal−oxygen bond (possible Fe−O stretching frequencies) vibrations for the perovskite-structure compound. TG-DTG confirms the formation temperature of SFO ranging between 850−900 °C. XRD results reveal that the use of mixture of fuels in the preparation has effect on the crystallite size of the resultant compound. The average particle size of the samples prepared from single fuels as determined from XRD was ∼50−35 nm, whereas for samples obtained from mixture of fuels, particles with a size of 30−25 nm were obtained. Specifically, the combination of mixture of fuels for the synthesis of SFO catalysts prevents agglomeration of the particles, which in turn leads to decrease in crystallite size and increase in the surface area of the catalysts. It was also observed that the present approach also impacted the catalytic activity of the SFO in the catalytic reduction of nitrobenzene to azoxybenzene.

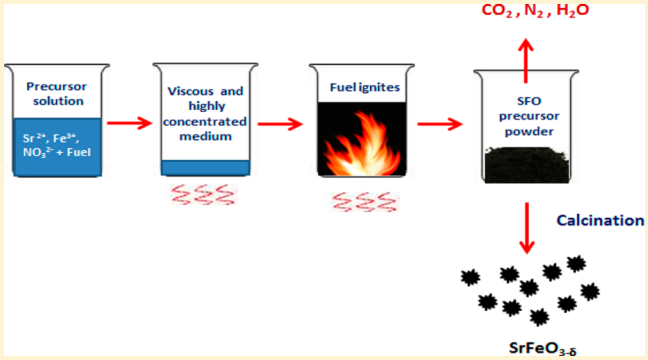

1. INTRODUCTION

Among ferrites, strontium ferrite $SrFeO_{3-\delta}$ ($0 < \delta < 0.5$) perovskite has attracted increasing attention due its strong oxygen-deficient composition for various applications. This wide range of nonstoichiometry, implying different oxidation states for iron cations, and the presence of oxygen vacancies make this system very attractive for catalysis, for instance, for methane combustion[1] and oxidative dehydration of ethane.[2] $SrFeO_{3-\delta}$ has also been used as an electrode material in solid oxide fuel cell and has been considered as a possible candidate for high-temperature solid-state electrochemical devices in particular as dense oxygen separation membranes for partial oxidation of methane to syngas.[3−6] Teraoka and co-workers[7] have shown that substituted $SrCo_xFe_{1-x}O_{3-\delta}$ has exceptionally high oxygen-transport rates, and thus the interest in these materials is increasing. The nonstoichiometric chemistry of this system, which can also be traced back to the different synthesis routes used for its preparation, has been thoroughly investigated, and four distinct compounds with nominal compositions of $Sr_nFe_nO_{3n-1}$ (n = 2, 4, 8, and ∞) have been structurally described.[8]

Traditionally, $SrFeO_{3-\delta}$ has been prepared by conventional solid-state reaction of Fe_2O_3 and SrO in the temperature range of 1000−1200 °C.[9] This conventional solid-state reaction process suffers from many disadvantages such as high reaction temperature, large particle size formation, loss of chemical homogeneity, and low sinterability. Different synthetic approaches have been optimized to prepare ferrites, such as solvothermal,[10] hydrothermal synthesis,[11] forced hydrolysis,[12] water-in-oil (w/o) inverse microemulsion,[13] citric acid precursor method,[14] microwave-assisted coprecipitation,[15] and liquid-phase deposition,[16] by exploiting the decomposition of suitable single-source precursors[17] and by coprecipitation methods.[18] However, to the best our knowledge, there are no reports on the synthesis of $SrFeO_{3-\delta}$ using solution-combustion synthesis process. A wide variety of inorganic materials has been prepared using solution-combustion process.[19] It is fast and simple compared to other methods of synthesis and yields high-purity, homogeneous, crystalline oxides in a short preparation time and with less net energy input. In this approach, the physical properties such as surface area, particle size distribution, and agglomeration of the particles in the final product depend on the flame temperature, which in turn

Received: August 31, 2014
Published: November 3, 2014

   dx.doi.org/10.1021/ic502121k | *Inorg. Chem.* 2014, 53, 12178−12185

depends on the nature of fuel and fuel to oxidant ratio. In solution combustion synthesis, the type and amount of the fuel plays an important role in determining the morphology, composition, and particulate properties of the final product. Mixture of fuels approach facilitates the reduction in particle size compared to the product formed using single fuel.[20] Overall mixture of fuels approach gives a good control over flame temperature. Specifically, there are no reports available on using mixture of fuels for the synthesis of $SrFeO_{3-\delta}$ by solution combustion method.

The synthesized $SrFeO_{3-\delta}$ catalysts have been evaluated for the catalytic reduction of nitrobenzene to azoxybenzene. Azoxy compounds have received much attention because of their physiological activities and utilization in liquid crystal systems.[21] Azoxybenzenes (AZYs) have been utilized as dyes, analytical reagents, reducing agents, stabilizers, and polymerization inhibitors. The most common approach for the synthesis of AZY is the reduction of aromatic nitro compounds by a variety of homogeneous and heterogeneous catalysts. These methods include reduction of nitrobenzene with glucose/NaOH,[22] sodium arsenate,[23] Mg reagent,[24] KBH_4,[25] PH_3,[26] and yellow phosphorus.[27] Thallium-mediated reduction[28] of nitrobenzene is reported as a well-known method for the synthesis of AZY. Zinc in the presence of acetic acid and acetic anhydride,[29] Se,[30] and Te[31] reagents were used as suitable reagents for nitrobenzene conversion. Recently, we have reported Fe-doped $BaTiO_3$ as a highly efficient catalyst for the catalytic reduction of nitrobenzene to synthesize AZY.[32] In the present study, we synthesized for the first time $SrFeO_{3-\delta}$ nanocatalysts by solution combustion process using combination of mixture of fuels and applied these catalysts for the catalytic reduction of nitrobenzene to AZY. The above catalysts were characterized using Fourier transform infrared (FT-IR) spectroscopy, X-ray diffraction (XRD), thermogravimetric analysis and derivative thermogravimetric analysis (TG-DTG), scanning electron microscopy (SEM), transmission electron microscopy (TEM), and N_2 physisorption methods, and their acidic strength was assessed by potentiometric titration method.

2. EXPERIMENTAL SECTION

Synthesis of $SrFeO_{3-\delta}$ by Solution Combustion Method. The starting materials used in this study are $Sr(NO_3)_2{\cdot}6H_2O$ (Sigma-Aldrich), $Fe(NO_3)_3{\cdot}9H_2O$ (Merck), oxalic acid (Merck), citric acid (Merck), and glycine (Merck). Stoichiometric amounts of oxidants such as strontium nitrate hexahydrate (0.2M), iron nitrate nonahydrate (0.2M), and the fuel, for example, citric acid (0.4M), respectively, were dissolved in minimum quantity of water, and the formed solution was kept on a hot plate preheated at 180 °C; the solution boils, foams, catches fire, and burns with an incandescent flame to yield $SrFeO_{3-\delta}$ (SFO) precursor with the evolution of gases as reported in the literature.[13] Finally, the prepared precursor was ground to a fine powder and calcined at 900 °C for 12 h in a static air furnace. The fuel and the oxidant (metal nitrates) molar ratio in the reaction mixture was maintained at unity. A stoichiometric composition is defined as the composition where ratio of oxidizing to reducing valency is equal to unity and ensures that the evolution of heat is maximized. List of the samples prepared by the above-described method and their fuel compositions are given in Table 1.

3. CATALYST CHARACTERIZATION

The crystallinity and phase identification of the powders was determined by using Philips X-ray diffractometer (X'pert MPD 3040) with Cu Kα as radiation source. The average crystallite size was obtained by line-broadening method using Scherrer and Warren formula:

$$D = \frac{0.9\lambda}{(B^2 - b^2)^{1/2}\cos\theta}$$

where D is the crystallite size, λ the wavelength of the radiation, θ the Bragg's angle, and B and b are the full width at half maxima (fwhm) observed for the sample and standard, respectively.

FT-IR spectra were measured on a PerkinElmer FT-IR-300 spectrometer using KBr pellet method. The Brunauer–Emmett–Teller (BET) surface area of the samples was measured using a Model-Quantachrome Autosorb iQ_2 automated gas sorption analyzer. Samples were initially pretreated in N_2 at 300 °C for 4 h, and the BET surface area and pore volume of the catalysts were obtained by adsorbing N_2 at liquid nitrogen temperature, −196 °C.

The TG-DTG analysis was carried out on a Mettler-Toledo apparatus. In a typical experiment, sample weight of 10–20 mg was analyzed in the N_2 flux in the temperature ranging from 25 to 1000 °C and at a heating rate of 10 °C/min.

The acidic strength of the solid samples was measured by the potentiometric titration method. A known mass of solid suspended in acetonitrile was stirred for 3 h, and the suspension was titrated with a solution of 0.05 N *n*-butylamine in acetonitrile, at a flow rate of 0.02 mL/min; the variation in the electrode potential was measured with a potentiometric titrator using a standard calomel electrode. The acidity of the catalyst measured by this technique enables determination of the total number of acidic sites and their strength. To interpret the results, it is suggested that the initial electrode potential (E_i) be taken as maximum acidic strength of the surface sites and the range; where the plateau is reached (meq/g) can be considered as the total number of acid sites. The acidic strength of the surface sites can be assigned according to the following ranges[33] very strong site $E_i > 100$ mV; strong site $0 < E_i < 100$ mV; weak site $-100 < E_i < 0$ mV; very weak site $E_i < -100$ mV.

Field emission scanning electron microscope (FESEM), model INSPECTTM S50, was used for morpholological studies. TEM model JEM-2010, JEOL, Tokyo, Japan, was used to study the morphology of the sample.

Table 1. List of $SrFeO_{3-\delta}$ Samples Prepared and Their Fuel Compositions

sample name	fuel composition
SFO-1	0.4 M citric acid (CA)
SFO-2	0.4 M oxalic acid (OA)
SFO-3	0.4 M glycine (Gly)
SFO-4	0.2 M oxalic acid + 0.2 M citric acid
SFO-5	0.2 M citric acid + 0.2 M glycine
SFO-6	0.2 M oxalic acid + 0.2 M glycine
SFO-7	0.134 M oxalic acid + 0.134 M citric acid + 0.134 M glycine

4. CATALYTIC ACTIVITY

Catalytic reduction with propan-2-ol as hydrogen donor was carried out under continuous stirring in a two-necked 100 mL round-bottom flask fitted with a reflux condenser with H_2 gas bubbling through the reaction mixture. Analysis was done by withdrawing definite aliquots of the sample at regular intervals. In a typical experiment, 150 mg of the catalyst was dispersed in a solution containing 20 mmol of nitrobenzene, 20 mmol of KOH pellets, and 20 mL of propan-2-ol. The mixture was

dx.doi.org/10.1021/ic502121k | Inorg. Chem. 2014, 53, 12178–12185

stirred and heated under reflux for 2−6 h in an oil bath in the presence of H_2 gas. The products were analyzed on the basis of their retention times using a gas chromatograph-mass spectrometer.

5. RESULTS AND DISCUSSION

5.1. X-ray Diffraction. Figure 1 shows the indexed powder XRD patterns of $SrFeO_{3-\delta}$ calcined powders at 900 °C for 12 h.

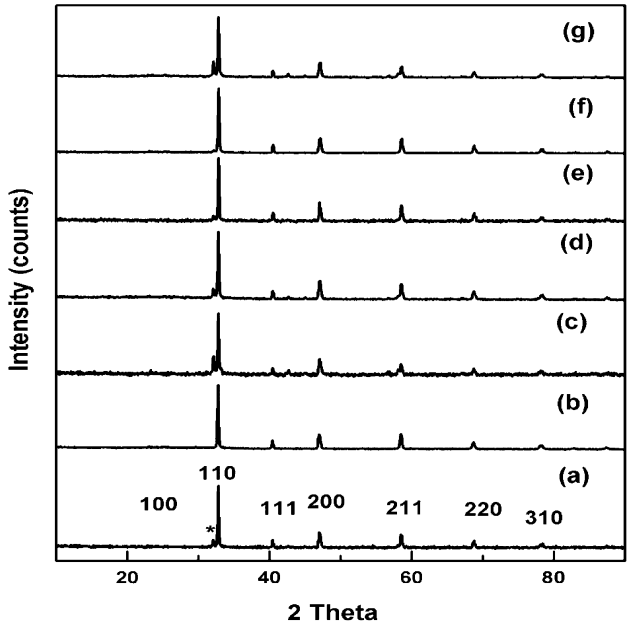

Figure 1. XRD patterns of the SFO samples calcined at 900 °C. (a) SFO-1 (b) SFO-2 (c) SFO-3 (d) SFO-4 (e) SFO-5 (f) SFO-6 (g) SFO-7; *$Sr_4Fe_3O_{10-x}$.

$SrFeO_{2.97}$ phase with cubic symmetry and $Pm\bar{3}m$ space group is observed in all the samples and confirmed the same by comparing the d values with the standard JCPDS Pattern No. 040−0905. Traces of $Sr_4Fe_3O_{10-x}$ at corresponding $2\theta = 32.14°$ was found as minor phase in all the samples except in the sample prepared with oxalic acid (SFO-2). It indicates that the oxalic acid is the suitable fuel for obtaining the pure phase of $SrFeO_{3-\delta}$. The average crystallite size calculated from XRD line broadening is shown in Table 3. It is observed from the table that the crystallite size of the samples decreased with mixture of fuels compared to the single fuels. It was reported that[20] mixture of fuels prevents the agglomeration of particles, and combustion reaction will take place at lower temperatures than the single fuels. This leads to decrease in average crystallite size of the samples.

5.2. FT-IR Spectroscopy of SFO Samples at Various Temperatures. FT-IR spectra of as-synthesized samples are shown in Figure 2(I). The IR bands in the region of 1350−1460 cm^{-1} correspond to the symmetric NO_2 and asymmetric stretching vibration of nitrate group. The less-intense bands that appeared in the region of 810−820 cm^{-1} are due to N−O stretching, and bands at 700−740 cm^{-1} are due to NO_2 bending vibrational mode of strontium nitrate phase present in the SFO samples. Infrared vibrations corresponding to traces of Fe_3O_4 at 564 cm^{-1} and $SrCO_3$ at 862 cm^{-1} were also observed in the spectra.

FT-IR spectra of SFO samples calcined at 900 °C measured in the range of 400−2000 cm^{-1} are shown in Figure 2(II).The spectra of all the SFO samples showed a broad absorption band in the region of 590−599 cm^{-1} correspond to Fe−O stretching vibration. The broad band contains shoulder at 545 cm^{-1}. This indicates the formation of $SrFeO_{3-\delta}$, and it was reported that the appearance of the two bands was due to defective $SrFeO_{3-\delta}$ compound formation. This defect structure arises due to production of oxygen vacancies by Sr^{2+}.[34]

During the thermal treatment of the strontium ferrite precursor at temperatures up to 450 °C the major crystalline phase present is strontium nitrate. This can be designated as stage 1. Heating the precursor at 600 and 700 °C produces strontium carbonate as well as iron oxide (Fe_3O_4). This can be termed as stage 2. The final stage, stage 3, gives the formation

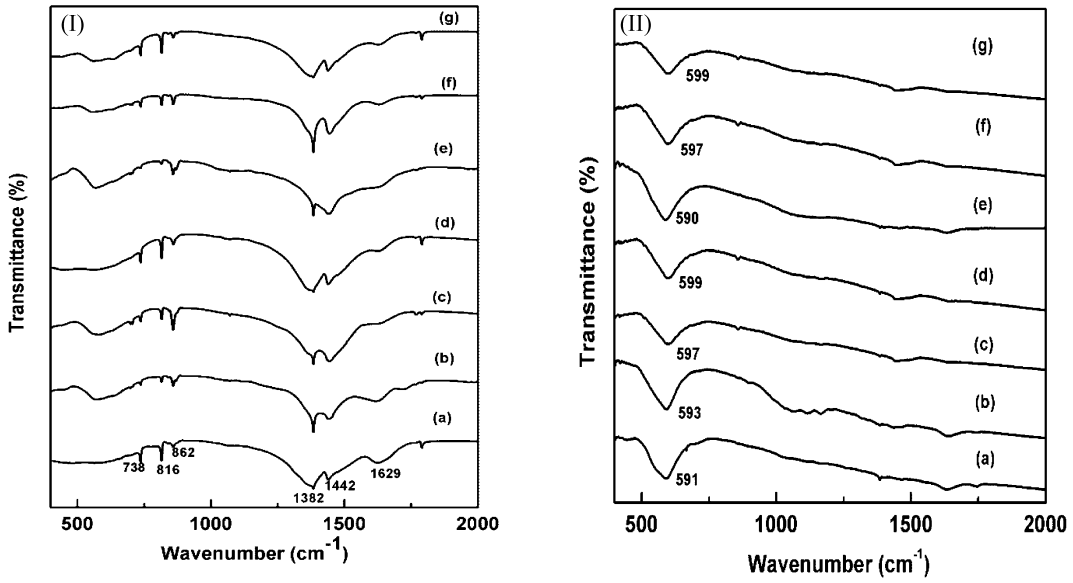

Figure 2. FT-IR spectra of SFO (I) as-synthesized samples and (II) calcined at 900 °C. (a) SFO-1 (b) SFO-2 (c) SFO-3 (d) SFO-4 (e) SFO-5 (f) SFO-6 (g) SFO-7.

dx.doi.org/10.1021/ic502121k | Inorg. Chem. 2014, 53, 12178−12185

Table 2. FTIR Phase Identification of the SFO Samples Calcined at Various Temperatures

sample	temperature (°C)	phase[a] identification	IR band position (cm^{-1})
SFO-1 to 7	ambient	$Sr(NO_3)_2$	1629 (w), 1382 (vs), 1442 (m), 816 (w,sh), 738 (w,sh)
		Fe_3O_4 (traces)	561(m)
		$SrCO_3$ (traces)	862 (vw)
SFO-1, 3, 5, 6, 7	200	$Sr(NO_3)_2$	1634 (w), 1385 (vs), 1444 (m)
		Fe_3O_4 (traces)	560−585 (m)
		$SrCO_3$ (traces)	858 (m,sh), 706, and 698 (vw)
SFO-2, 4	200	$Sr(NO_3)_2$	1627 (m), 1438 (w), 1384 (vs), 815 (w,sh), 732 (w,sh)
		Fe_3O_4 (traces)	564
SFO-1, 4, 5, 6	300	$Sr(NO_3)_2$	1633 (m), 1447 (w), 1384 (vs)
		Fe_3O_4 (traces)	530−565 (w)
		$SrCO_3$ (traces)	856, 695−707 (vw)
SFO-2, 3, 7	300	$Sr(NO_3)_2$	1632 (m), 1445 (w), 1384 (s,sh), 815 (w,sh), 737 (w,sh), 531(w, b)
SFO-1, 5	450	$SrCO_3$	1635 (w), 1447 (vs), 1385 (w,sh), 858 (m,sh), 699 (w)
		Fe_3O_4	560 (m)
SFO-2 to 4 and 7		$Sr(NO_3)_2$	1636 (m), 1454 (m), 1384 (v,s), 698, 736 (vw)
		Fe_3O_4	561 (m)
		traces of $SrCO_3$	857 (w, sh)
SFO-6		$Sr(NO_3)_2$	1631, 1384, 584
SFO-1 to 7	600	$SrCO_3$	1631(w), 1455 (vs), 1385 (vw), 858 (m,sh), 699, 705 (vw)
		Fe_3O_4	570 (m)
SFO-6	600	$Sr(NO_3)_2$	1633 (w), 1455 (m), 1384 (vs)
		traces of $SrCO_3$	859 (w,sh)
		Fe_3O_4	555 (m)
SFO-1 to 7	700	$SrCO_3$	1456 (s), 857 (m,sh), 698−705 (vw)
		Fe_3O_4	570−580 (m)
SFO-1 to 7	900	$SrFeO_{3-\delta}$	590−599 (b, m), 545 (sh)

[a]Phases identified according to reference FT-IR spectra of the corresponding compounds (Figure S1 given in Supporting Information).

of the required ferrite on heating the sample to temperatures of 900 °C. Table 2 summarizes the FTIR spectra of the products observed at various temperatures and their IR band positions. Explanations of the reaction mechanisms involved in each of the three stages from the thermal decomposition/oxidation are given below.

Table 3. Physical Properties of the Various SFO Materials

catalyst	BET surface area (m^2/g)	pore volume (mL/g)	acidic strength (meq/g)	XRD crystallite size (nm)	SEM particle size (nm)
SFO-1	27	0.0048	170	49.4	240
SFO-2	34	0.0064	169	46.9	270
SFO-3	58	0.0105	230	35.4	03−210
SFO-4	47	0.0087	122	29.0	03−250
SFO-5	30	0.0049	181	30.4	02−302
SFO-6	52	0.0112	110	27.7	06−280
SFO-7	60	0.013	195	26.2	03−290

Stage 1: FTIR analysis of samples heat treated from ambient to 450 °C (Figure 2(I) and Figure S2 given in Supporting Information). The SFO precursor powders at room temperature showed strontium nitrate as the main crystalline phase and traces of Fe_3O_4 and $SrCO_3$. In samples produced at 200, 300, and 450 °C the presence of the strontium nitrate is still evident except in the samples of SFO-1 and SFO-5made at 450 °C where strontium carbonate ($SrCO_3$) and iron oxide (Fe_3O_4) present as major crystalline phases, which indicate the beginning of decomposition of the strontium nitrate.

Stage 2: FT-IR analysis of the samples heat treated at 600 and 700 °C. (Figure S2, Supporting Information) The FT-IR analysis of samples produced by heat treatment at 600 and 700 °C showed the presence of iron oxide (Fe_3O_4) and the formation of strontium carbonate ($SrCO_3$). At 600 °C strontium nitrate has disappeared totally to form strontium carbonate product, which is either produced by reaction of strontium oxide formed from decomposition of strontium nitrate or direct reaction of strontium nitrate with CO_2 evolved during combustion of fuels or by interaction with atmospheric CO_2 to yield the carbonate as given in (eq 1).

Stage 3: FTIR and XRD at higher temperatures, 900 °C (Figures 1 and 2(II)). The samples obtained at 900 °C showed the presence of $SrFeO_{3-\delta}$ as major diffraction pattern and $Sr_3Fe_4O_{10-x}$ as a trace compound in most of the samples. It is evident that at these higher temperatures the strontium carbonate has decomposed according to equation given below. The SrO has subsequently reacted with the iron oxide Fe_3O_4 to produce the required ferrite. All the corresponding spectra of the SFO samples calcined from 200 to 700 °C are given in the Supporting Information.

$$SrCO_3(s) \rightarrow SrO(s) + CO_2(g)$$

5.3. Scanning Electron Microscopy. Figure 3 shows the SEM images of all the SFO samples. Because of their magnetic properties, highly dense microstructure exhibiting considerable agglomeration is apparent in all the samples. In general, spherical particles with homogeneous size distribution are observed in all the samples. The grain size of the samples calculated from SEM is given in Table 3 and is in the range of 210−302 nm. Hexagonal platelike structures were observed in the SFO-7 sample, which was synthesized using mixture of all three fuels. Hexagonal platelike formation was further confirmed with TEM analysis of SFO-7 sample (Figure 3h).

dx.doi.org/10.1021/ic502121k | Inorg. Chem. 2014, 53, 12178−12185

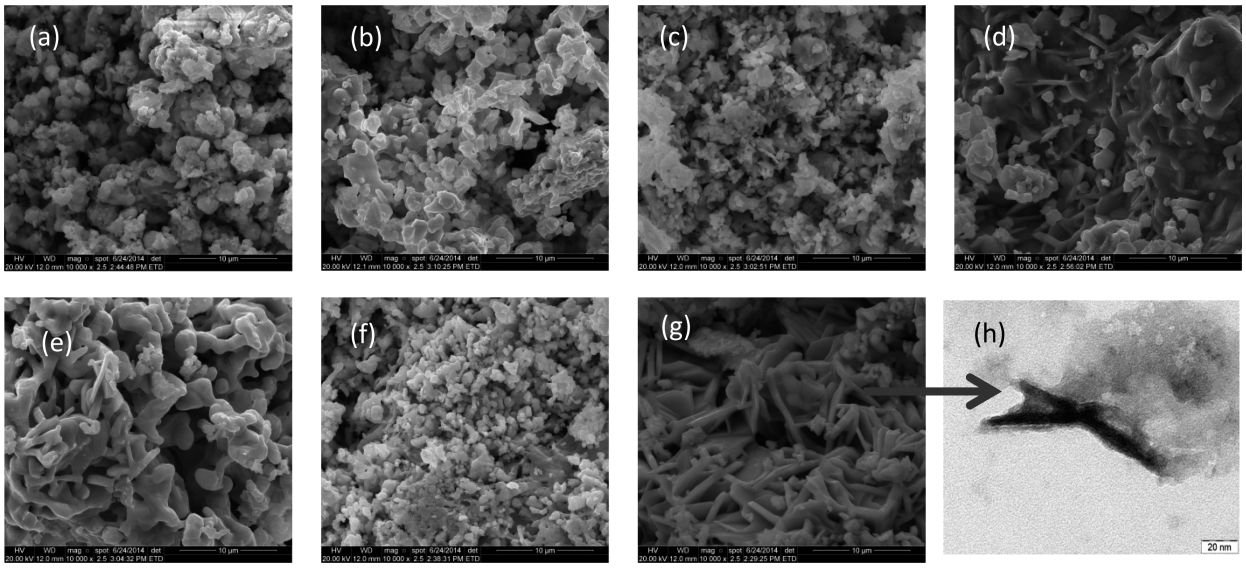

Figure 3. SEM images of the various SFO materials. (a) SFO-1 (b) SFO-2 (c) SFO-3 (d) SFO-4 (e) SFO-5 (f) SFO-6 (g) SFO-7 (h) TEM image of one platelet of SFO-7.

5.4. Thermogravimetric and Derivative Thermogravimetric Analysis. TG-DTG curves of the SFO precursor samples with a heating rate of 10 °C/min in nitrogen atmosphere are shown in Figure 4a−e. The TG curves of the SFO precursor samples exhibit four distinct weight loss steps. The first weight loss observed from ambient to 205 °C is attributed to the loss of absorbed water. The second weight loss from 280 to 370 °C observed mainly in Figure 4a,e and the corresponding endothermic peak in DTG at 360 °C could be due to decomposition of organics, and the third weight loss observed between 430 and 580 °C showed a sharp decrease due to decomposition of strontium nitrate into strontium carbonate. This was confirmed with the FT-IR analysis of the samples heat treated from 450 to 900 °C (see Table 2). Formation of $SrCO_3$ from strontium nitrate proceeds either by interaction of strontium nitrate with CO_2 evolved during organics decomposition or by interaction with atmospheric CO_2 as follows (eq 1)

$$Sr(NO_3)_2 + CO_2 \rightarrow SrCO_3 + 2NO_2 + 1/2O_2 \quad (1)$$

$$SrCO_3 \rightarrow SrO + CO_2 \quad (2)$$

$$Fe_3O_4 + 3SrO + O_2 \rightarrow 3SrFeO_{3-\delta} \quad (3)$$

The final weight loss, observed above 850 °C, was due to decomposition of strontium carbonate into SrO (eq 2), and subsequent reaction with Fe_3O_4 in the presence of O_2 leads to the formation of $SrFeO_{3-\delta}$ compound (eq 3). The changes observed in the TG-DTG of the samples are in good agreement with the FT-IR results of the samples heat treated from 200 to 900 °C.

5.5. Catalytic Reduction of Nitrobenzene. The catalytic reduction of nitrobenzene to AZY is illustrated in Scheme 1. The activity profiles of nitrobenzene obtained over various $SrFeO_{3-\delta}$ catalysts are shown in Figure 5. It was observed that conversion of nitrobenzene was low with SFO catalysts prepared by using single fuels and in the range of 67−80% compared to SFO catalysts obtained from mixture of fuels where conversion obtained was in the range of 80−91%. It can be observed from Figure 6 that the increase in conversion is independent of the acidic strength of the catalysts as the decrease in acidic strength of the catalysts does not have any impact on the conversion of nitrobenzene.

Selectivity toward AZY was found to increase in the catalysts obtained from mixture of fuels. The increase in selectivity is mainly due to increase in surface area and pore volume of the catalysts as given in Table 3. Selectivity obtained over SFO catalysts prepared from single fuels was in the range of 72−74% whereas the selectivity obtained over SFO catalysts prepared from mixture of fuels was between 75 and 82%. The raise in selectivity could also be due to decrease in acidic strength of the catalysts. It clearly indicates that the formation of AZY requires redox nature of the catalysts, which can be readily tuned via mixing of fuels during catalyst preparation. Mixing of fuel approach also prevents the agglomeration of the particles, which was evidenced by increase in surface area of the catalyst as well as pore volume (Table 3). The increase in selectivity is also in good agreement with the decrease in crystallite size of the catalysts obtained from XRD.

It can be inferred from the above results that the slight decrease in selectivity of the catalysts prepared with single fuels is due to formation of aniline as side product due to high acidic strength of the catalysts (Figure 6, SFO-1 to SFO-3) compared with SFO catalysts (Figure 6, SFO-4 to 7) obtained from mixture of fuels. It seems that the decrease in acidic strength might favor the coupling reaction between nitrosobenzene and hydroxylamine intermediates, leading to the formation of AZY. Mechanism of the reaction has been discussed in our previous paper (ref 32).

6. CONCLUSIONS

Nanocrystalline $SrFeO_{3-\delta}$was synthesized using single and mixture of various fuels by solution combustion method. The synthesis of nanocrystalline $SrFeO_{3-\delta}$ using the mixture of citric acid, glycine, and oxalic as fuels influenced the morphology, microstructure, and crystallite size of the samples. Various intermediate phases formed during heat treatment of the SFO precursors at various temperatures to transform to $SrFeO_{3-\delta}$ were identified using FT-IR spectroscopy. TG-DTG and FT-IR analyses confirm that strontium carbonate completely decomposed to SrO at temperatures above 825 °C, which

dx.doi.org/10.1021/ic502121k | Inorg. Chem. 2014, 53, 12178−12185

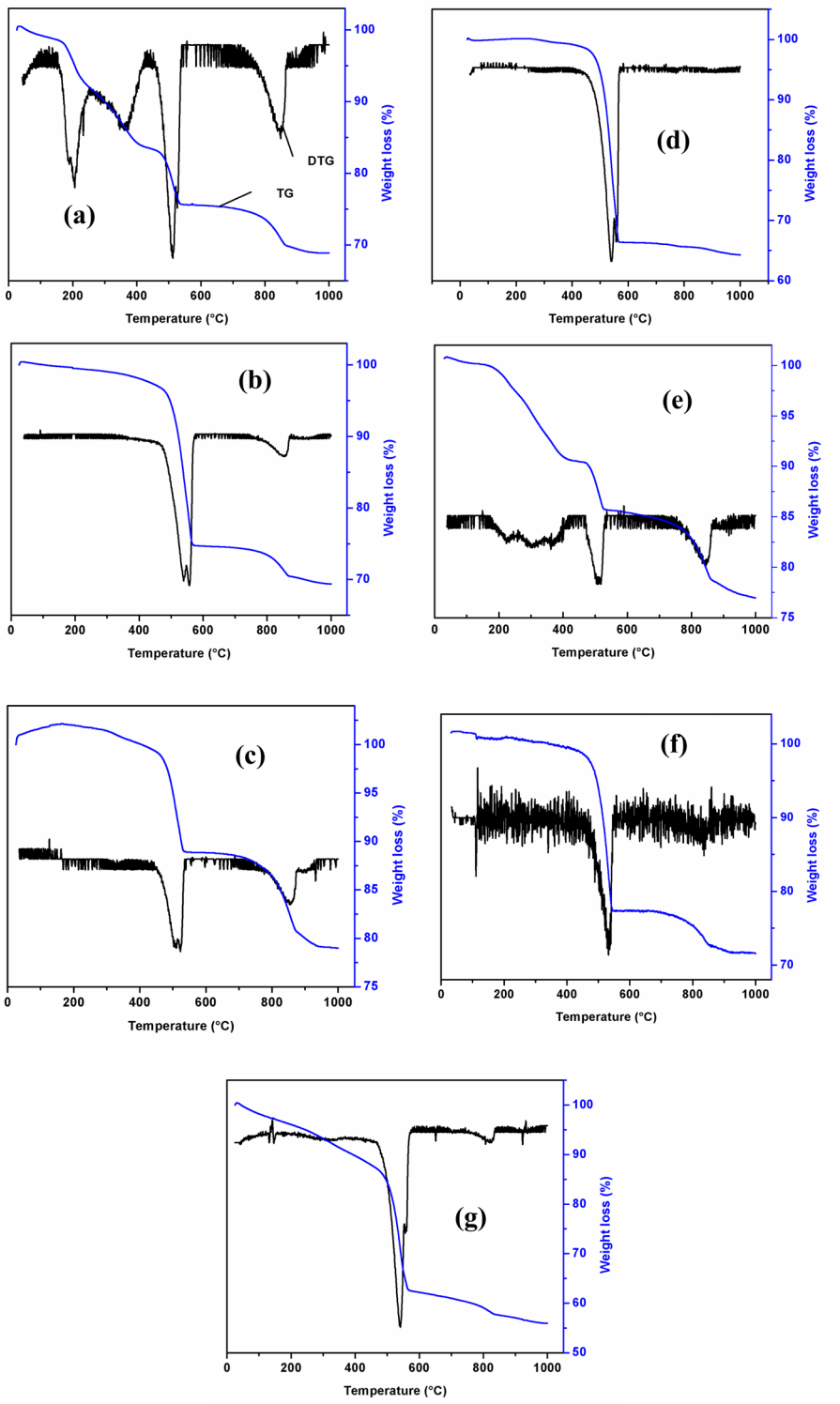

Figure 4. TG and DTG curves of SFO precursor samples. (a) SFO-1 (b) SFO-2 (c) SFO-3 (d)SFO-4 (e) SFO-5 (f) SFO-6 (g) SFO-7.

Scheme 1. Catalytic Reduction of Nitrobenzene to AZY

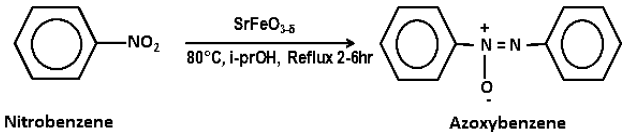

subsequently reacts with Fe_3O_4 to form strontium ferrite. XRD studies confirm that pure phase of $SrFeO_{3-\delta}$ can be obtained with oxalic acid as fuel. High surface area and pore volume of $SrFeO_{3-\delta}$ catalysts obtained from mixture of fuels could be due to prevention of agglomeration of particles and leads to a combustion reaction that will take place at lower temperatures than that of the single fuels. A crystallite size of 26 nm was achieved with the sample prepared from combination of three fuels. Thus, it is concluded that by using mixture of fuels one can not only reduce the exothermicity of the combustion reaction but also reduce the particle size to a greater extent.

dx.doi.org/10.1021/ic502121k | *Inorg. Chem.* 2014, 53, 12178−12185

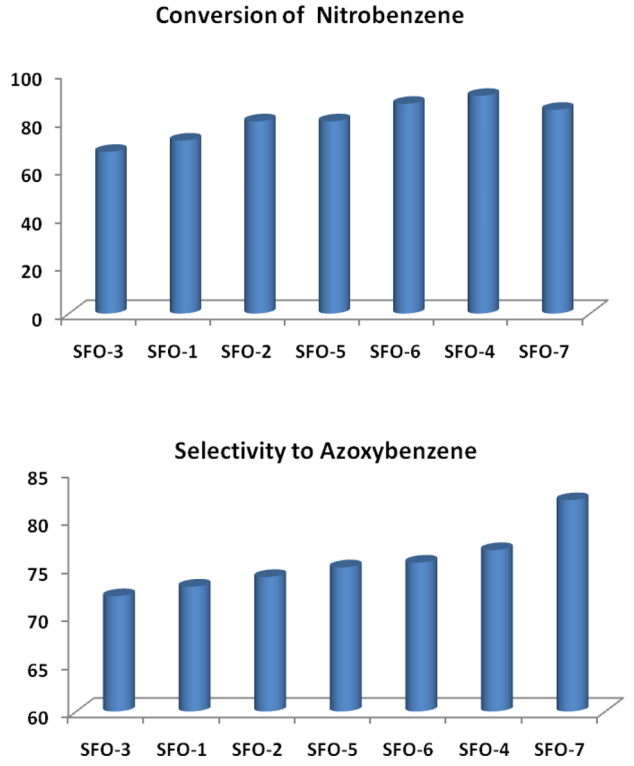

Figure 5. Activity profiles of the SFO catalysts for catalytic reduction of nitrobenzene to AZY.

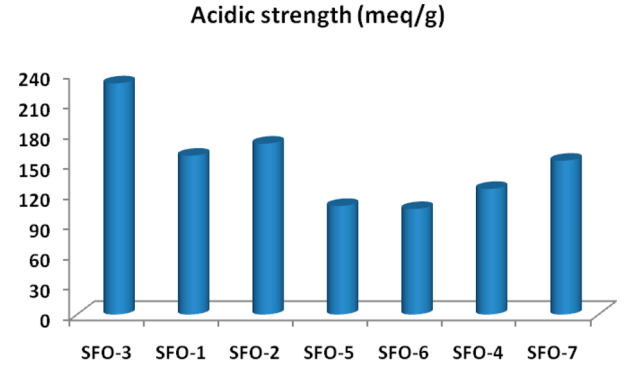

Figure 6. Acidic strength of the SFO catalysts obtained by *n*-butylamine titration method.

The mixture of fuel approach also has impact on the catalytic reduction of nitrobenzene and achieved good nitrobenzene conversion and AZY selectivity compared to $SrFeO_{3-\delta}$ catalyst prepared from single fuels.

■ ASSOCIATED CONTENT

Ⓢ Supporting Information

FTIR spectra of pure authentic samples is given in Figure S1, and FTIR spectra of the various SFO samples heat treated at various temperatures are given in Figure S2. This material is available free of charge via the Internet at http://pubs.acs.org.

■ AUTHOR INFORMATION

Corresponding Author

*E-mail: ch.srilakshmi@sscu.iisc.ernet.in.

Notes

The authors declare no competing financial interest.

■ ACKNOWLEDGMENTS

C.S.L. wishes to thank to department of Science and Technology for financial support through INSPIRE Faculty award.

■ REFERENCES

(1) Falcon, H.; Barbero, J. A.; Alonso, J. A.; Martınez-Lope, M. J.; Fierro, J. L. G. *Chem. Mater.* **2002**, *14*, 2325−2333.
(2) Dai, H. X.; Ng, C. F.; Au, C. T. *Catal. Lett.* **1999**, *57*, 115−120.
(3) Yoo, J.; Verma, A.; Wang, S.; Jacobson, A. J. *J. Electrochem. Soc.* **2005**, *152*, A497−A505.
(4) Zaspalis, V.; Evdou, A.; Nalbandian, L. *Fuel* **2010**, *89*, 1265−1273.
(5) Niu, Y.; Zhou, W.; Sunarso, J.; Ge, L.; Zhu, Z.; Shao, Z. *J. Mater. Chem.* **2010**, 209619−209622.
(6) Teraoka, Y.; Zhang, H. M.; Furukawa, S.; Yamazoe, N. *Chem. Lett.* **1985**, 1743−1746.
(7) Balachandran, U.; Morissette, S. L.; Picciolo, J. J.; Dusek, J. T.; Poeppel, R. B.; Pei, S.; Kleefisch, M. S.; Mieville, R. L.; Kobylinski, T. P.; Udovich, C. A. *International Gas Research Conference;* Thompson, H.A.; , Ed.; 1992, Vol. *2*, p 2499.
(8) Marchetti, L.; Forni, L. *Appl. Catal., B* **1998**, *15*, 179−187.
(9) Wang, Y.; Chen, J.; Wu, X. *Mater. Lett.* **2001**, *49*, 361−364.
(10) Yan, A.; Liu, X.; Shi, R.; Zhang, N.; Yi, R.; Li, Y.; Gao, G.; Qiu, G. *Solid State Commun.* **2008**, *146*, 483−486.
(11) Jiao, X.; Chen, D.; Hu, Y. *Mater. Res. Bull.* **2002**, *37*, 1583−1588.
(12) Duong, G. V.; Hanh, N.; Linh, D. V.; Groessinger, R.; Weinberger, P.; Schafler, E.; Zhetbauer, M. *J. Magn. Mater.* **2007**, *311*, 46−50.
(13) Grasset, F.; Labhsetwar, N.; Li, D.; Park, D. C.; Saito, N.; Haneda, H.; Cador, O.; Roisnel, T.; Mornte, S.; Duguet, E.; Portier, J.; Etourneau, J. *Langmuir* **2002**, *18*, 8209−8216.
(14) Lee, J. C.; Caruntu, D.; Lee, J. H.; Kim, J. J.; Cushing, B.; Golub, V.; ChoS, H.; O'Connor, C. J. *Funct. Mater.* **2006**, *13*, 447−456.
(15) Bensebaa, F.; Zavliche, F.; L'Ecuyer, P.; Cochrane, R. W.; Veres, T. *J. Colloid Interface Sci.* **2004**, *277*, 104−110.
(16) Yourdkhani, A.; Caruntu, G. *J. Mater. Chem.* **2011**, *21*, 7145−7153.
(17) Zhao, J.; Mi, L.; Hu, H.; Shi, X.; Fan, Y. *Mater. Lett.* **2007**, *61*, 4196−4198.
(18) Tirosh, E.; Shemer, G.; Markovich, G. *Chem. Mater.* **2006**, *18*, 465−470.
(19) Rao, C. N. R. Combustion Synthesis. In *Chemical Approaches to the Synthesis of Inorganic Materials;* Wiley Eastern Limited: New Delhi, 1994, 28−30.
(20) Aruna, S. T.; Kini, N. S.; Rajam, K. S. *Mater. Res. Bull.* **2009**, *44*, 728−733.
(21) Snyder, J. P.; Bandurco, V. T.; Darack, F.; Olsen, H. *J. Am. Chem. Soc.* **1974**, *96*, 5158−5166 and references cited therein.
(22) Degering, E. F.; Hitch, E. F. *J. Am. Chem. Soc.* **1951**, *73*, 1323−1324.
(23) Bigelow, H. E.; Palmer, A. *Org. Synth.* **1943**, *2*, 57−59.
(24) Zechmeister, L.; Rom, P. *Justus Liebigs Ann. Chem.* **1929**, *468*, 117−132.
(25) Shine, H. J.; Mallory, H. E. *J. Org. Chem.* **1962**, *27*, 2390−2391.
(26) Buckler, S. A.; Doll, L.; Lind, F. K.; Epstein, M. *J. Org. Chem.* **1962**, *27*, 794−798.
(27) Kozlov, N. S.; Soshin, V. A. *Uch. Zap. Permsk. Gos. Pedagog. Inst.* **1965**, *32*, 84; *Chem. Abstr.* **1967**, *66*, 2290k.
(28) McKillop, A.; Raphael, R. A.; Taylor, E. C. *J. Org. Chem.* **1970**, *35*, 1670−1672.
(29) Cullen, E.; L'Ecuyer, P. *Can. J. Chem.* **1961**, *39*, 862−869.
(30) Osuka, A.; Shimizoo, H.; Suzuki, H. *Chem. Lett.* **1983**, 1373−1374.
(31) Ohe, K.; Takahoshi, H.; Uemura, S.; Sugita, N. *J. Chem. Soc., Chem. Commun.* **1988**, 591−592.
(32) Srilakshmi, Ch.; Vijayakumar, H.; Praveena, K.; Shivakumara, C.; Muralidhar Nayak, M. *RSC Adv.* **2014**, *4*, 18881−18884.

(33) Srialkshmi, Ch.; Lingaiah, N.; Suryanarayana, I.; Sai Prasad, P. S.; Ramesh, K.; Anderson, B. G.; Niemantsverdriet, J. W. *Appl. Catal., A* **2005**, *296*, 54−62.
(34) Augustin, C. O.; John Berchmans, L.; KalaiSelvan, R. *Mater. Lett.* **2004**, *58*, 1260−1266.